Influence of the Water/Titanium Alkoxide Ratio on the Morphology and Catalytic Activity of Titania–Nickel Composite Particles for the Hydrolysis of Ammonia Borane

Tetsuo Umegaki,*[a] Yoshifumi Yamamoto,[a] Qiang Xu,[b] and Yoshiyuki Kojima[a]

This work reports the influence of the water/titanium alkoxide ratio during the preparation of titania–nickel composite particles on their morphology and catalytic activity toward the hydrolysis of ammonia borane. The titania–nickel composite particle catalysts were fabricated by using a sol-gel method, followed by an activation process in aqueous solution containing sodium borohydride and ammonia borane. From the scanning electron microscopy images and pore-size distributions calculated from nitrogen sorption data, the particle dispersion was significantly enhanced at ratios above 6000, and increased with increasing water/titanium alkoxide ratio. Stoichiometric amounts of hydrogen were evolved in the presence of all of the prepared titania–nickel composite particle catalysts. The particle dispersion influenced the hydrogen evolution rate from aqueous ammonia borane solution, and the samples with the most highly dispersed particles showed the highest hydrogen evolution rate. The most active catalyst showed an apparent activation energy comparable to that of other reported catalysts and high cycle ability for the hydrolysis of ammonia borane.

1. Introduction

Secure storage and effective release of hydrogen remains one of the major technological barriers for the widespread application of hydrogen energy.[1,2] Currently, considerable efforts are being devoted to the search for suitable hydrogen storage materials including metal hydrides, sorbent materials, and chemical hydrides.[3] Among them, ammonia borane (NH_3BH_3) has attracted much attention as a hydrogen carrier for portable hydrogen storage applications, owing to its high gravimetric hydrogen density (19.6 wt%), high stability and solubility under ambient conditions, environmentally friendliness, and favorable kinetics for hydrogen release.[4–6] In the presence of suitable catalysts, ammonia borane releases hydrogen via hydrolysis under ambient conditions. Therefore, the development of catalysts able to boost the kinetics of hydrogen generation through ammonia borane hydrolysis is highly relevant for both academia and industry.

The hydrolysis of ammonia borane in the presence of a catalyst has been well investigated. Noble-metal-based catalysts, such as those incorporating Au, Ru, Pt, Rh, and Ir, have shown highly efficient hydrogen generation from aqueous ammonia borane solution under mild conditions; however, their low abundance and high price hamper their industrial application.[7–11] Meanwhile, low-cost and resourceful catalysts based on transition metals (Fe, Co, Ni, and Cu) have also been studied.[12–23] The catalytic performance of metal nanoparticles and composite particles containing metals is highly dependent on the dispersion of the active metals and/or composite particles.[18,24] For example, our research group found that the Si+Ni content influences the dispersion of silica–nickel composite particles and their catalytic activity for the hydrolytic dehydrogenation of ammonia borane.[18] The results also indicated that the ratio of water to silicon alkoxide influences the dispersion and activity of the catalyst.

In the present study, we have investigated the influence of the preparation conditions on the dispersion and catalytic activity of titania–nickel composite particle catalysts toward hydrogen evolution from aqueous ammonia borane. We have previously reported that titania–nickel composite catalysts show higher activity for the hydrolysis reaction than silica–nickel composite catalysts.[17] To improve their dispersion, we focused on the control of the titanium alkoxide sol-gel reaction equilibrium, and then investigated the influence of the water/titanium alkoxide ratio on the dispersion of the titania–nickel composite particle catalysts and their activity for the hydrolysis of ammonia borane.

[a] Dr. T. Umegaki, Y. Yamamoto, Prof. Dr. Y. Kojima
Department of Materials & Applied Chemistry
College of Science & Engineering, Nihon University
1-8-14, Kanda-Surugadai, Chiyoda-Ku, Tokyo 101-8308 (Japan)
E-mail: umegaki.tetsuo@nihon-u.ac.jp

[b] Prof. Dr. Q. Xu
National Institute of Advanced Industrial Science and Technology (AIST)
1-8-31, Midorigaoka, Ikeda, Osaka (Japan)

The ORCID identification number(s) for the author(s) of this article can be found under:
https://doi.org/10.1002/open.201800116.

2. Results and Discussion

The morphology of the titania–nickel composite particle catalysts prepared at varying water/titanium alkoxide molar ratios was studied by TEM imaging (Figure 1). The sample prepared
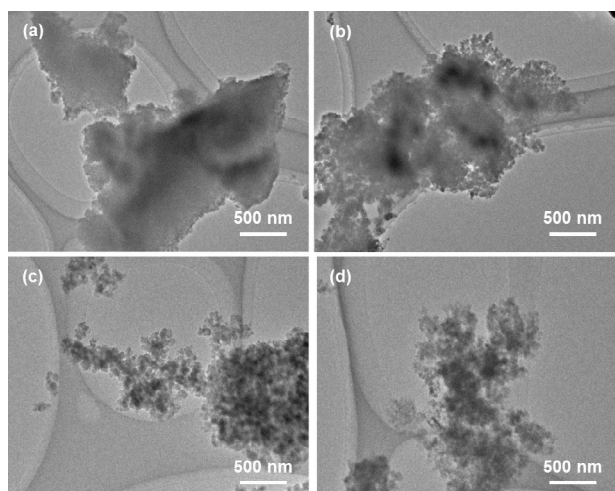

Figure 1. TEM images of the titania–nickel composite particle catalysts prepared at water/titanium alkoxide ratios of a) 3000, b) 6000, c) 9000, and d) 12 000, after the activation process.

with a water/titanium alkoxide molar ratio of 3000 consisted of 1–3 μm aggregates, including fine primary particles with a diameter of up to 100 nm (Figure 1 a). The fine primary particles were found to be uniformly dispersed at ratios of over 6000, where their dispersion improved with the increasing water/titanium alkoxide molar ratio (Figure 1 b–d). Such enhanced dispersion with the increasing ratio was also confirmed by nitrogen sorption measurements. All the physicochemical properties (specific surface area, pore volume, and average pore diameter) were significantly enhanced at ratios over 6000, also increasing with the increasing ratio (Table 1). The results of their pore-size distributions also reflect this tendency. The diameter of the mesopores and macropores of the samples significantly increased at water/titanium alkoxide molar ratios of 6000, further increasing with the water/titanium alkoxide molar ratio (Figure 2). The preparation process of the titania–nickel composite particles is based on a sol-gel reaction, which consists of the hydrolysis of titanium alkoxide into titanium hy-

Table 1. Physicochemical properties of the titania–nickel composite particle catalysts prepared at different water/titanium alkoxide ratios.

H$_2$O/titanium alkoxide	S_{BET} [m^2 g^{-1}][a]	V [cm^3 g^{-1}][b]	D [nm][b]
3000	56.7	0.0755	5.31
6000	79.6	0.2448	12.05
9000	71.0	0.2847	16.47
12 000	83.5	0.3182	15.32

[a] Brunauer–Emmett–Teller (BET) surface area. [b] Calculated from the adsorption branch of their nitrogen adsorption-desorption isotherms.
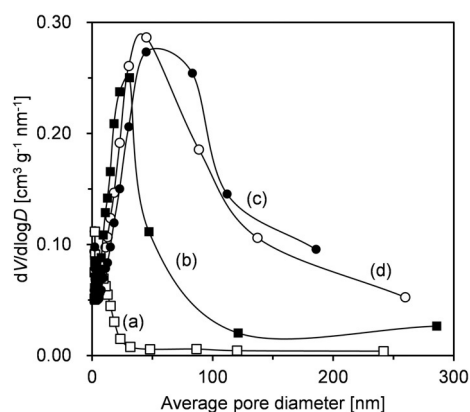

Figure 2. Pore-size distributions of the titania–nickel composite particle catalysts prepared at water/titanium alkoxide ratios of a) 3000, b) 6000, c) 9000, and d) 12 000.

droxide and its subsequent condensation (Figure 3). Conventionally, particles are prepared at water/titanium alkoxide ratios of the order of ten through sol-gel-based methods.[25–28] On
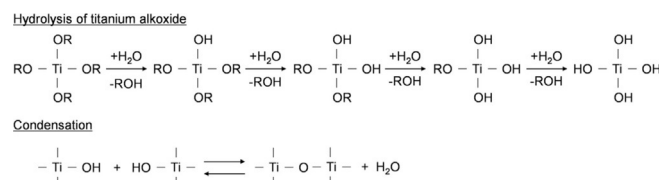

Figure 3. Scheme of the preparation process based on a sol-gel reaction.

the other hand, the water/titanium alkoxide molar ratios in the present study were 10^2–10^3 times higher than those employed under conventional preparation conditions. These results indicate that the condensation reaction equilibrium is suppressed with significantly large amounts of water relative to the titanium alkoxide content. As shown in high resolution TEM images (Figure 4), the morphology of the catalysts did not significantly change before and after the activation process.

The valence state of the active nickel species in the titania–nickel composite particle catalysts was characterized by DRUV/Vis absorption spectroscopy before and after the activation process in aqueous solution containing sodium borohydride and ammonia borane (Figure 5). In the spectra of the precursors, the observed absorption bands at 550–650 nm can be attributed to the electronic transition $^3T_{1g}(F) \leftarrow {}^3A_{2g}(F)$ for Ni^{2+},[29] indicating that all the precursors contain Ni^{II} with octahedral coordination.

Compared to the spectra of each precursor, the intensity of the peaks in the spectra after the activation process was negligible. The results indicate that active metallic nickel species were obtained in all samples through the activation process. Figure 6 shows the XPS spectra of the sample prepared at a water/titanium alkoxide ratio of 12 000. The spectrum of the titania–nickel composite particle precursor exhibits a Ni 2p$_{3/2}$ band at 855.6 eV, typical of Ni^{2+}.[22] On the other hand, Ni 2p$_{3/2}$ bands at 856.2 and 852.5 eV are observed in the spectrum of
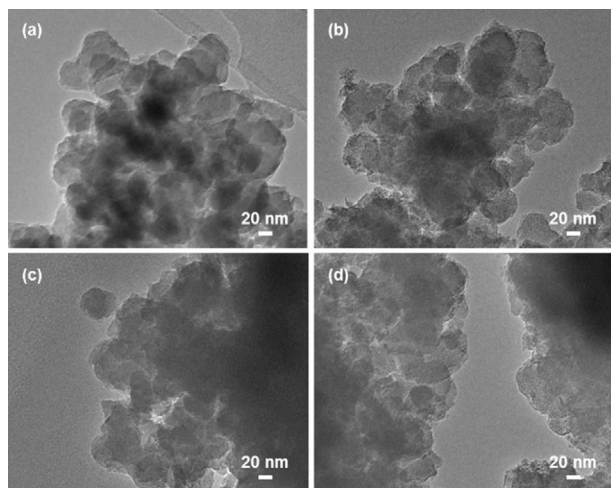
Figure 4. High-resolution TEM images of the titania–nickel composite particle catalyst prepared at water/titanium alkoxide ratio of a, b) 9000 and c, d) 12 000 before (a, c) and after (b, d) the activation process.
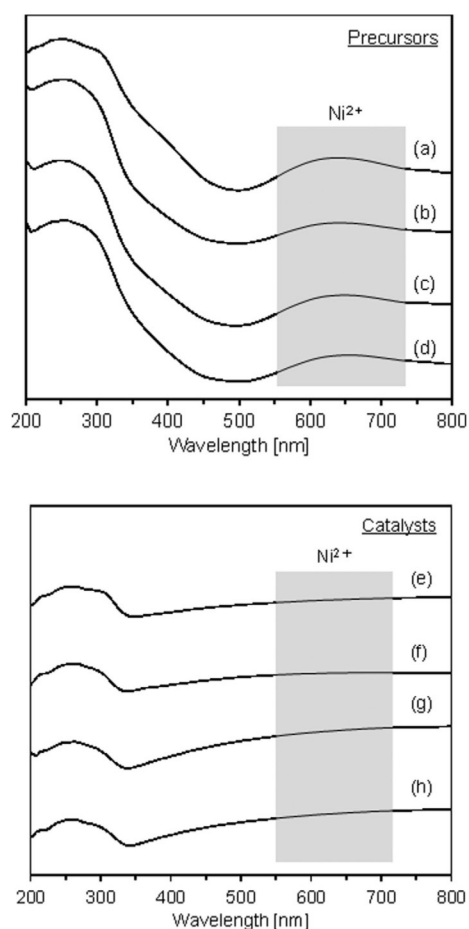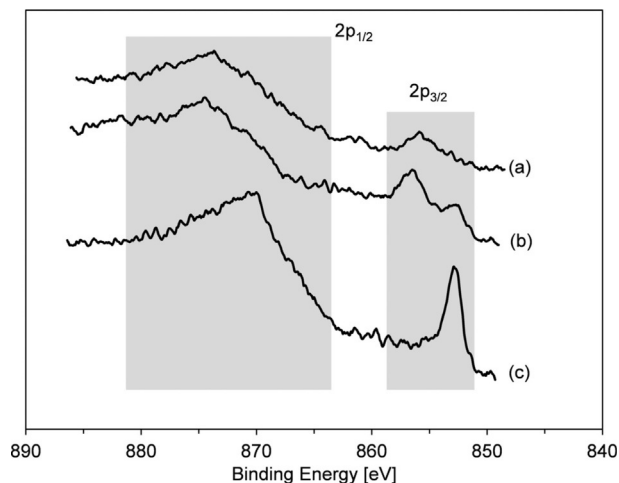

Figure 6. XPS spectra of the titania–nickel composite particles prepared at a water/titanium alkoxide ratio of 12 000: a) precursor, b) catalyst, c) catalyst after Ar$^+$ sputtering for 5 min.

Figure 5. DRUV/Vis spectra of the titania–nickel composite particles prepared at water/titanium alkoxide ratios of a, e) 3000, b, f) 6000, c, g) 9000, and d, h) 12 000 before (a–d) and after (e–h) the activation process in aqueous solution containing sodium borohydride and ammonia borane.

the titania–nickel composite particle catalyst, which are typical of Ni^{2+} and metallic Ni^0, respectively.[22] The results indicate that some nickel species exist on the surface of the titania–

nickel composite particles, and that part of such nickel species were oxidized after the activation process, probably owing to exposure to air before XPS measurement. To identify the valence state of nickel species inside the titania–nickel composite particles, the spectrum of the titania–nickel composite particle catalyst was obtained after Ar$^+$ sputtering. The spectrum in Figure 6 c exhibits only a Ni 2p$_{3/2}$ band at 852.7 eV, which is typical of metallic Ni^0. The results indicate that the nickel species inside the titania–nickel composite particles do not oxidize in air, but maintain their metallic state.

The evolution of hydrogen from aqueous ammonia borane solution in the presence of the composite particle catalysts was evaluated. Figure 7 shows the time course of the hydrogen evolution from aqueous solution in the presence of the catalysts prepared at different water/titanium alkoxide ratios. A hydrogen evolution of 59.0, 60.0, 59.0, and 60.0 mL from the aqueous ammonia borane solution was completed within ap-
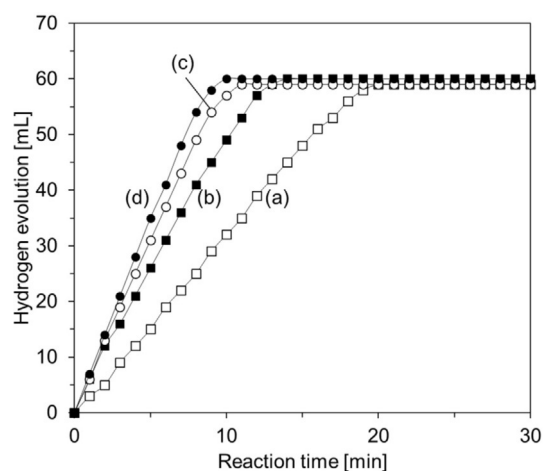

Figure 7. Hydrogen evolution from the hydrolysis of ammonia borane catalyzed by the titania–nickel composite particle catalysts prepared at water/titanium alkoxide ratios of a) 3000, b) 6000, c) 9000, and d) 12 000.

proximately 20, 14, 11, and 10 min in the presence of the catalysts prepared at water/titanium alkoxide ratios of 3000, 6000, 9000, and 12 000, respectively. Hydrogen is produced from aqueous ammonia borane via Reaction (1):

$$NH_3BH_3 + 2H_2O \rightarrow NH_4^+ + BO_2^- + 3H_2 \qquad (1)$$
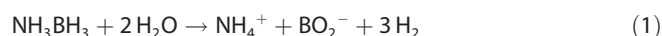
Under the present reaction conditions, approximately 59 mL of hydrogen (24.0×10^{-4} mol) was generated through this reaction. The molar ratio of the hydrolytically generated hydrogen to the initial ammonia borane in the presence of the titania–nickel composite particle catalyst was determined as 3.0. The results indicate that stoichiometric amounts of hydrogen were evolved in the presence of the different titania–nickel composite particle catalysts, because the reducibility of the active nickel species is very similar in all the catalysts. On the other hand, the hydrogen evolution rate was found to depend on the catalyst; the rate in the presence of the titania–nickel composite particle catalysts prepared at water/titanium alkoxide ratios of 3000, 6000, 9000, and 12 000 was 3.33, 5.00, 6.00, and 6.67 mL min^{-1}, respectively. These results, in addition to those shown in Figures 1 and 2 and Table 1, indicate that the catalyst with the most highly dispersed primary particles shows the highest hydrogen evolution rate, probably because of a higher diffusion rate of the reactants into the active sites.

The catalytic hydrolysis of ammonia borane was further evaluated with the titania–nickel composite particle catalyst prepared at a water/titanium alkoxide ratio of 12 000 at various temperatures in the range of 298–343 K, so as to determine the apparent activation energy [Eq. (2)].

$$-3d[NH_3BH_3]/dt = d[H_2]/dt = k \qquad (2)$$

where k is the reaction rate, [NH$_3$BH$_3$] and [H$_2$] are the amount of NH$_3$BH$_3$ and H$_2$, respectively. Under our experimental conditions, the reaction rate, k, is constant at each given temperature, implying zero order kinetics for the ammonia borane hydrolysis reaction. This suggests that the hydrogen generation rate is controlled by surface reactions. The reaction rate equation can be written as follows [Eq. (3)]:

$$k = k_0 \exp(-E_a/RT) \qquad (3)$$

where k_0 is the reaction constant (mL min^{-1}), E_a the activation energy for the reaction, R the gas constant, and T is the reaction temperature. Using Equation (3), the value of the rate constant k at different temperatures for the hydrolysis of ammonia borane was calculated from the linear segment of the time course of hydrogen evolution in the presence of the catalyst prepared at a water/titanium alkoxide ratio of 12 000 at different temperatures in the range of 298–343 K. The Arrhenius plots are shown in Figure 8. They were also used to calculate the activation energy parameter ($E_a = 37.5$ kJ mol^{-1}) for the catalyst. The obtained activation energy is comparable to that of other reported nickel-based catalysts.[21,30,31]
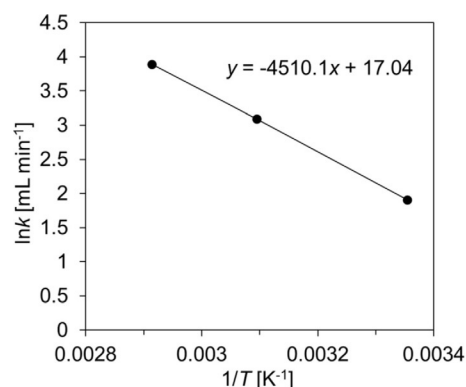

Figure 8. Arrhenius plots for the hydrolysis of ammonia borane catalyzed by the titania–nickel composite particle catalyst prepared at a water/titanium alkoxide ratio of 12 000.

Figure 9a shows the time course at the 1st, 5th, 9th, 11th, and 15th cycle for the hydrogen evolution from aqueous ammonia borane solution in air catalyzed by the titania–nickel composite particle catalyst prepared at a water/titanium alkox-
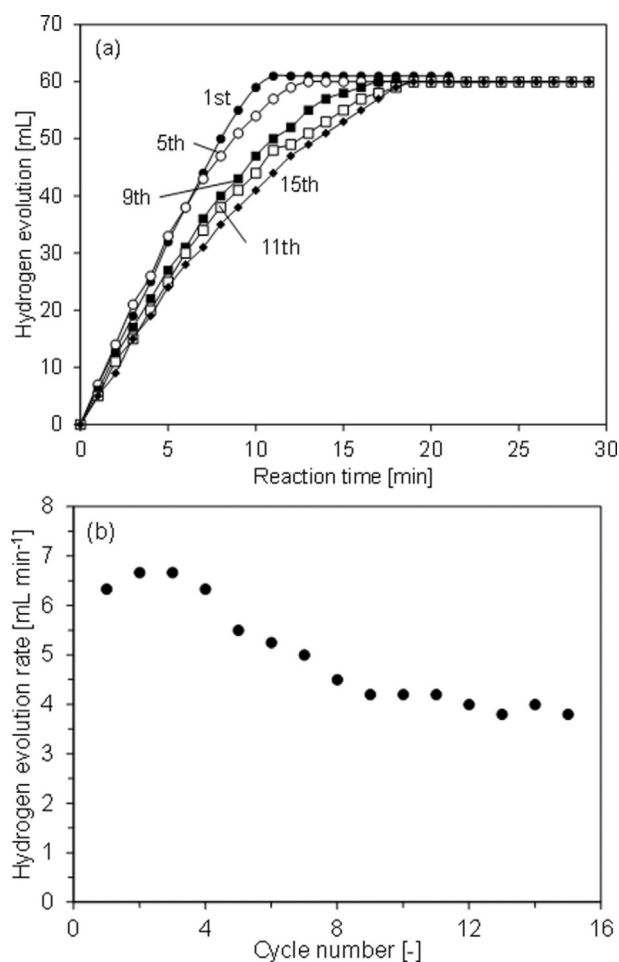

Figure 9. a) Time course for the evolution of hydrogen from aqueous ammonia borane solution catalyzed by the titania--nickel composite particle catalyst prepared at a water/titanium alkoxide ratio of 12 000 for the 1st, 5th, 9th, 11th, and 15th cycle and b) the hydrogen evolution rate at each cycle.

ide of 12 000. The amount of hydrogen evolution does not depend on the cycle, as approximately 60 mL of hydrogen was evolved in all cycles. The results indicate that stoichiometric amounts of hydrogen were evolved. On the other hand, the evolution rate was found to depend on the cycle number. The hydrogen evolution rate dropped significantly from the 5th to the 9th cycle, to then decrease further in a lesser way. Figure 9 b plots the hydrogen evolution rate against the cycle number. Up to the 4th cycle, the hydrogen evolution rate was stable at around 6.5 mL min^{-1}, whereas it decreased from the 5th to the 9th cycle. Then, the rate was maintained at approximately 4.0 mL min^{-1} up to the 15th cycle. From EDX measurements of the sample before activation process and after the 10th cycle, the nickel content included in the sample is 2.36 and 1.67 mol %, respectively. In addition, the peak assigned as Ni^{II} was not observed in the UV/Vis spectrum of the catalyst after 10th cycle. From these results, the active metallic nickel species remained in the catalyst, whereas a decrease in the hydrogen evolution rate is probably attributable to dissolution and/or oxidation of some of the active metallic nickel species on the surface of the titania–nickel composite particles.

3. Conclusions

The present work describes the influence of the water/titanium alkoxide ratio during the preparation of titania–nickel composite particle catalysts on their morphology and activity toward the hydrolysis of ammonia borane. From their TEM images and pore-size distributions, the dispersion of the particles was enhanced at ratios above 6000, increasing with increasing water/titanium alkoxide ratio. Stoichiometric amounts of hydrogen were evolved in the presence of all the prepared titania–nickel composite particle catalyst. The dispersion of the particles was found to influence the hydrogen evolution rate from the aqueous ammonia borane, and the sample with the most highly dispersed particles showed the highest hydrogen evolution rate. The most active catalyst showed a comparable apparent activation energy that other reported catalysts and high cyclability for 15 cycles.

Experimental Section

Catalyst Preparation

Titanium tetra-n-butoxide monomer [(C$_4$H$_9$O)$_4$Ti, 0.245 mL, Kanto Chem. Co., >97.0%] was dissolved in ethyl alcohol (27.2–133.6 mL), to which 35.4–141.8 mL of an aqueous solution containing nickel nitrite [Ni(NO$_3$)$_2$·6H$_2$O, 0.03 g, Wako Pure Chem. Ind. Ltd., >99.9%] and L(+)-arginine (C$_6$H$_{14}$N$_4$O$_2$, 0.0201 M, Wako Pure Chem. Ind. Ltd., >98.0%) was added. The mixed solution was stirred at 343 K for 24 h. The resulting product was filtrated and dried in a desiccator. The obtained powder (24.8 mg) was mixed with sodium borohydride (NaBH$_4$, 5 mg, Kanto Chemical Co., >98.5%) and ammonia borane (NH$_3$BH$_3$, 27.5 mg, Aldrich, 90%) (NH$_3$BH$_3$/NaBH$_4$/Ni = 1:0.17:0.05) in a two-necked round-bottomed flask. One neck was connected to a gas burette and the other was fitted with a septum inlet to introduce deionized water (5 mL). The reaction was started by addition of deionized water to the mixture of the catalyst pre-

cursor, sodium borohydride, and ammonia borane, and the activation process was carried out at 343 K in air.

Characterization

The morphology of the titania–nickel composite particle catalysts was observed on a Hitachi S-450 scanning electron microscope operating at an acceleration voltage of 15 kV. The physicochemical properties of the composite particles were evaluated by nitrogen sorption isotherms at 77 K on a Micromeritics Model ASAP 2010MC analyzer. Diffuse reflectance ultraviolet and visible (DRUV/Vis) spectra were recorded over the range of 200–800 nm to identify the valence state of the nickel species in the samples on a UV-3600 (Shimadzu Co. Ltd.). UV/Vis spectrophotometer using barium sulfate as the standard. X-ray photoelectron spectra were acquired on an ESCA-3400 spectrometer (Shimadzu Co. Ltd.) equipped with a Mg Kα X-ray excitation source (1253.6 eV) operating at 10 kV and 10 mA. The binding energies (BEs) are referenced to the C 1s peak at 285.0 eV.

Experimental Procedure for the Hydrolysis of Ammonia Borane

An aqueous ammonia borane solution (0.16 M, 5 mL) was added to the catalyst suspension after the activation process described above, and the evolution of gas was monitored at 298 K using the gas burette for the evaluation of the catalytic activity. The hydrogen evolution reaction was carried out at 298, 323 and 343 K for the assessment of the activation energy. For the cyclability tests, additional equivalents of said aqueous ammonia borane solution (0.16 M, 5 mL) were added to the reaction flask once the previous hydrogen evolution reaction was completed. Such cycles were carried out fifteen times in air.

Conflict of Interest

The authors declare no conflict of interest.

[1] L. Schlapbach, A. Züttel, *Nature* **2001**, *414*, 353–358.
[2] H. Yen, Y. Seo, S. Kaliaguine, F. Kleitz, *ACS Catal.* **2015**, *5*, 5505–5511.
[3] Q. L. Zhu, Q. Xu, *Energy Environ. Sci.* **2015**, *8*, 478–512.
[4] N. Wang, Q. Sun, R. Bai, X. Li, G. Guo, J. Yu, *J. Am. Chem. Soc.* **2016**, *138*, 7484–7487.
[5] M. Wen, Y. Cui, Y. Kuwahara, K. Mori, H. Yamashita, *ACS Appl. Mater. Interfaces* **2016**, *8*, 21278–21284.
[6] X. Du, C. Yang, X. Zeng, T. Wu, Y. Zhou, P. Cai, G. Chen, W. Luo, *Int. J. Hydrogen Energy* **2017**, *42*, 14181–14187.
[7] M. Chandra, Q. Xu, *J. Power Sources* **2007**, *168*, 135–142.
[8] E. K. Abo-Hamed, T. Pennycook, Y. Vaynzof, C. Toprakcioglu, A. Koutsioubas, O. A. Scherman, *Small* **2014**, *10*, 3145–3152.
[9] W. Chen, J. Ji, X. Feng, X. Duan, G. Qian, P. Li, X. Zhou, D. Chen, W. Yuan, *J. Am. Chem. Soc.* **2014**, *136*, 16736–16739.
[10] J. Shen, L. Yang, K. Hu, W. Luo, G. Cheng, *Int. J. Hydrogen Energy* **2015**, *40*, 1062–1070.
[11] C. Du, Q. Ao, N. Cao, L. Yang, W. Lou, G. Cheng, *Int. J. Hydrogen Energy* **2015**, *40*, 6180–6187.
[12] F. Y. Cheng, H. Ma, Y. Li, J. Chen, *Inorg. Chem.* **2007**, *46*, 788–794.
[13] X. J. Yang, F. Y. Cheng, J. Liang, Z. L. Tao, J. Chen, *Int. J. Hydrogen Energy* **2009**, *34*, 8785–8791.

[14] C. Cao, C. Chen, W. Li, W. Song, W. Cai, *ChemSusChem* **2010**, *3*, 1241–1244.

[15] Ö. Metin, V. Mazumder, S. Özkar, S. H. Sun, *J. Am. Chem. Soc.* **2010**, *132*, 1468–1469.

[16] T. Umegaki, C. Takei, Q. Xu, Y. Kojima, *Int. J. Hydrogen Energy* **2013**, *38*, 1397–1404.

[17] T. Umegaki, C. Takei, Y. Watanuki, Q. Xu, Y. Kojima, *J. Mol. Catal. A* **2013**, *371*, 1–7.

[18] T. Umegaki, A. Seki, Q. Xu, Y. Kojima, *J. Alloys Compd.* **2014**, *588*, 615–621.

[19] K. V. Manukyan, A. Cross, S. Rouvimov, J. Miller, A. S. Mukasyan, E. E. Wolf, *Appl. Catal. A* **2014**, *476*, 47–53.

[20] M. Yurderi, A. Bulut, I. E. Ertas, M. Zahmakiran, M. Kaya, *Appl. Catal. B* **2015**, *165*, 169–175.

[21] C. Tang, L. Xie, K. Wang, G. Du, A. M. Asiri, Y. Luo, X. Sun, *J. Mater. Chem. A* **2016**, *4*, 12407–12410.

[22] C. Wang, J. Tuninetti, Z. Wang, C. Zhang, R. Ciganda, L. Salmon, S. Moya, J. Ruiz, D. Astruc, *J. Am. Chem. Soc.* **2017**, *139*, 11610–11615.

[23] C. Tang, F. Qu, A. M. Asiri, Y. Luo, X. Sun, *Inorg. Chem. Front.* **2017**, *4*, 659–666.

[24] J. Wang, Y. L. Qin, X. Liu, X. B. Zhang, *J. Mater. Chem.* **2012**, *22*, 12468–12470.

[25] T. López, K. A. Espinoza, A. Kozina, P. Castillo, A. Silvestre-Albero, F. Rodriguez-Reinoso, R. Alexander-Katz, *Langmuir* **2011**, *27*, 4004–4009.

[26] M. González Hurtado, S. Pimenta Cheble Caplan, B. Guenther Soares, J. Rieumont Briones, K. Alfonso Alfonso, L. M. Castro, *J. Mater. Environ. Sci.* **2015**, *6*, 1554–1561.

[27] A. E. Danks, S. R. Hall, Z. Schnepp, *Mater. Horiz.* **2016**, *3*, 91–112.

[28] D. Brühwiler, H. Frei, *J. Phys. Chem. B* **2003**, *107*, 8547–8556.

[29] K. Hadjiivanov, M. Mihaylow, D. Klissurski, P. Stefanov, N. Abadjieva, E. Vassileva, L. Mintchev, *J. Catal.* **1999**, *185*, 314–323.

[30] J. Shen, N. Cao, Y. Liu, M. He, K. Hu, W. Luo, G. Cheng, *Catal. Commun.* **2015**, *59*, 14–20.

[31] Y. Du, K. Wang, Q. Zhai, A. Chen, Z. Xi, J. Yan, X. Kang, M. Chen, X. Yuan, M. Zhu, *Int. J. Hydrogen Energy* **2018**, *43*, 283–292.